Numerical Modeling of Powder Flow during Coaxial Laser Direct Metal Deposition – Comparison between Ti-6Al-4V Alloy and Stainless Steel 316L

S. Morville[1], M. Carin[*1], D. Carron[1], P. Le Masson[1], M. Gharbi[2], P. Peyre[2] and R. Fabbro[2]
[1]LIMATB, Université de Bretagne-Sud/UEB, [2]PIMM / UMR 8006 CNRS, Arts et Métiers Paris Tech
*Corresponding author: Centre de recherche C. Huygens, rue de Saint Maudé, BP 92116 Lorient, FRANCE, muriel.carin@univ-ubs.fr

Abstract: This paper presents a 3D numerical model to predict the whole process of coaxial powder flow, including the particle stream flow in and below the nozzle and also the laser-particle interaction process. The Particle Tracing Module of Comsol Multiphysics® is used to solve the coupled momentum transfer equations between the particle and gas phase while incorporating particle temperature evolution. A turbulence k-ε model is employed to describe the behavior of the gas flow. The trajectory of the discrete phase particle is calculated by integrating the force balance on each particle while taking into account gravity and drag forces. Heating of powder particles accounts for laser intensity, convection and radiation losses. The powder concentration and particle heating process are analyzed for two materials: Ti-6Al-4V alloy and 316L stainless steel. The influence of laser power distribution is analyzed. The numerical results are compared with experimental data.

Keywords: direct metal deposition, coaxial nozzle, powder flow, laser, heat transfer and fluid flow

1. Introduction

Direct Metal Laser Deposition (DMLD) has received significant attention due to its diversified potential. In this process, a thin layer is obtained through melting metallic powder coaxially delivered on the substrate. The layer-by-layer deposition of the material makes it possible to produce 3D metal objects of complex shapes. However, the quality and efficiency of DMLD largely depend on the powder stream structure below the nozzle. The development of numerical models has proven useful for improving the process. In the past decade, many analytical and numerical models have been developed by researchers, revealing the process dependences on related parameters. Pinkerton [1] proposed an analytical model of the powder stream and particle heating using the geometry of the nozzle. No account was taken of the particle drag and loss of momentum. More realistic models have been developed taking into account the interaction between gas flow and particle stream. These models use generally a turbulent two-phase flow model solved with the software FLUENT. This has been done by Lin [2] and Zhu [3] for a two-dimensional axial symmetry model and Zekovic [4] who proposed a 3D model. However, beam attenuation and powder heating were not considered in these works. Ibarra-Medina [5] has proposed a single fully-coupled model of laser cladding process. This model simultaneously calculates the powder motion by gas drag and collisions with nozzle and substrate walls, thermal interactions between the powder stream and laser beam, particle catchment and ricocheting, melt pool formation and melt pool flows, heat transfer from powder to melt pool and mass addition. The volume of fluid method is applied to determine the free surface of the clad. In this work, the commercial code CFD-ACE+ is used. Tabernero [6] has recently proposed a 3D model of powder stream. This model estimates the attenuation suffered by the laser beam due to the interaction with the powder flow during the laser cladding process. This model is calibrated and validated experimentally for two different materials. However, the reported literature does not include much work on the improvement of surface finish.

In this paper, a numerical model is developed to predict metal powder flow in coaxial nozzle for DMLD. This model is used to better understand the influence of the operating parameters on the surface finish. The Particle Tracing Module of Comsol Multiphysics® is chosen to solve the coupled momentum transfer equations between the particle and gas phase while incorporating particle temperature

evolution. The powder concentration and particle heating process are analyzed for two materials: Ti-6Al-4V alloy and 316L stainless steel. The influence of the distribution of the laser beam is studied. The choice of 2D axial symmetry or 3D geometry is discussed. The numerical results are compared with experimental data.

2. Governing equations

A schematic of the DMLD process is shown in Fig. 1. The metal powder is injected through a coaxial nozzle into a melt pool obtained by a moving laser beam. With laser scanning, the melt solidifies rapidly and a track is formed. The whole part is obtained by the layer-by-layer deposition of the material. A continuous wave disk Yb:YAG laser is used as a heat source.

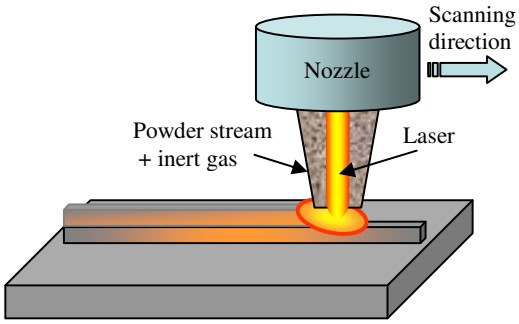

Figure 1. Schematic of DMLD process.

The gas flow at the nozzle exit is produced by the combination of argon streams from the central, middle and outer channels. The central and outer gas streams ensure the optics protection and oxidation protection respectively. In the middle inlet, argon is used as a driving gas, in order to convey the powder to the melt pool (Fig. 2). The shape of the nozzle is chosen in order to produce a converging annular stream of powder particles which are focused towards the substrate. Indeed, travelling along the nozzle, particles collide with the nozzle walls. These collisions determine the concentration distribution and dispersion of particles. After exiting the nozzle, the powder particles are drawn downward by the action of gravity and drag force from the different gas flows. The time and the spatial characteristics of the interaction between the powder and the laser beam are critical for the process. Indeed this interaction determines how much additional thermal energy the particles will bring when hitting the melt pool. The present model simulates the gas flow and heat transfer phenomena occurring in the powder stream. The computational domain comprises the inner geometry of the nozzle annular channels and the space between the nozzle exit and the substrate. The first step starts by calculating the gas flow. As the powder particles volume fraction is less than 10%, a dilute gas-particle stream is assumed. This assumption allows the application of one-way coupled discrete phase modelling. During the second step, the motion of the particles is determined. Finally, the heating of powder particles is treated using a lumped capacitance approach.

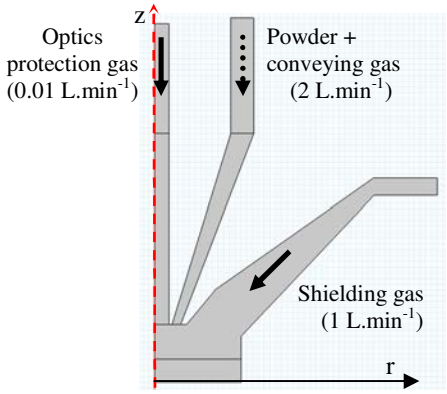

Figure 2. 2D axial-symmetry geometry for powder flow model

2.1 Gas flow

The steady turbulent gas flow in the powder stream is described by the standard k-ε model. In such model, the governing equations for laminar flows are modified using the time-averaging method known as Reynolds averaging. All the equations can be found in [2-4]. The values of the empirical constants describing the turbulent model are taken from the default values proposed by COMSOL Multiphyscis®. The equations are expressed with a compressible formulation (Mach number < 0.3), as recommended by Kovalev et al [7].

2.2 Powder stream

Immersed in the surrounding gas, each particle is treated by the Lagrangian approach. Discrete phase model is used to solve each particle's dynamic behavior. Particles are driven by the forces of gas flow drag and gravity. This force balance equates the particle inertia with the forces acting on the particle, and can be written as:

$$\frac{du_{p,i}}{dt} = \frac{18\mu}{\rho_p d_p^2}\frac{C_D Re}{24}\left(u_{g,i} + \xi\sqrt{\frac{2k}{3}} - u_{p,i}\right) + \frac{g_i(\rho_p - \rho_g)}{\rho_p}$$

where ρ_p, d_p, $u_{p,i}$ are the density, diameter, and velocity in the i-direction of each particle, respectively. ρ_g, μ and $u_{g,i}$ represent the density, the dynamic viscosity and the velocity in the *i* direction of the gas, respectively. *Re* is the Reynolds number, g_i is the i-component of gravity force. C_D is the drag coefficient and is detailed in [8]. A shape factor of 0.8 is assumed to account for non-spherical particles, which is classical when the particles are obtained by gas atomization. The additional term $\xi\sqrt{2k/3}$ gives a random motion of the particle which represents turbulent effects. The parameter ξ is a normally distributed random number with zero mean and unit standard deviation and k is the turbulent kinetic energy. No collision between each two particles is considered due to the very low powder feed rate. The particles are injected randomly at each time step. To describe the size distribution of particles comprised between 45 and 75 µm, a Normal low is considered for both materials (stainless steel 316L and Ti-6Al-4V alloy).

During their flight, the particles will travel through the laser irradiation zone where they are heated up. The heating of powder particles is modeled using the lumped capacitance approach, as the Biot number is less than 0.1. To consider the process of phase change for a particle, the energy equation is proposed as follows:

$$m_p c_p^*(T)\frac{dT_p}{dt} = I_l \eta_p \pi r_p^2 - h(T_p - T_\infty)4\pi r_p^2 - \varepsilon\sigma(T_p^4 - T_\infty^4)4\pi r_p^2$$

where m_p is the particle mass, c_p* is the equivalent specific heat capacity which includes the latent heat, T_p and r_p are the temperature and the radius of a particle, respectively. I_l denotes the laser intensity, η_p the particle absorptivity of laser power, ε the emissivity of particle, σ the Stefan-Boltzmann constant, and T_∞ the temperature of the surrounding gas. *h* is the convective heat transfer coefficient, which is determined from Nusselt number correlations [8]. This coefficient depends on the gas and particle velocities. The material properties are taken from [9] and [10] for 316L and Ti-6Al-4V alloys respectively. The gas properties for argon come from [11].

Two laser distributions are studied: an uniform and a Gaussian distributions. The uniform distribution is given by:

$$I_l = \frac{P_{laser}}{\pi r_{laser}^2}$$

where P_{laser} represents the laser power (320 W) and r_{laser} is the radius of the laser beam (0.65 mm).

The Gaussian distribution is as follows:

$$I_l = \frac{N P_{laser}}{\pi r_{laser}^2}\exp\left(-N\frac{r^2}{r_{laser}^2}\right)$$

with N = 5.

The values of N and r_{laser} have been obtained using a laser beam analyzer.

Concerning the boundary conditions of the turbulent problem, velocity is set for the three inlets based on the experimental gas flow rates (Fig. 2). Wall function is chosen for the interior walls of the nozzle and the substrate surface. An open boundary is set for the lateral boundary between the substrate and the nozzle exit. A condition of symmetry is applied for the other boundaries.

Concerning the problem of particle flow, an inlet condition is chosen for the middle channel entry. A powder feed rate of 1 $g.min^{-1}$ for both materials is used. An outlet condition with a "freeze" wall condition is set for the substrate surface and a "disappear" wall condition for the lateral outlet. A "bounce" wall condition is chosen for all the walls of the nozzle.

The calculations are performed using Particle Tracing Module and CFD Module. The computation time for the 3D model is around 3 hours (4 x 3.33 GHz, 96 Go RAM) using linear tetrahedral finite elements of 0.5 mm for the boundaries and 1 mm inside the domain.

3. Results and discussion

Figure 3 depicts the simulated powder stream structure formed by multi-particle trajectories for 316L and Ti-6Al-4V alloys. At the nozzle exit, the particles have a convergent trajectory for both materials. The particle streams merge into a main stream to form a waist, at a distance of 6.6 mm below the nozzle tip for the 316L steel and 9.9 mm for the Ti-6Al-4V alloy. After traveling further distance, the main stream diverges. The difference between focus plane locations is due to a higher particle mass for 316L steel. The heavier particles are less influenced by the axial gas flow and reach the nozzle axis at a higher position than the Ti-6Al-4V particles. Note that the gas velocities and particle size are identical for both materials. Moreover, in order to obtain the same powder feed rate, the number of injected particles for 316L steel is reduced. It is worth to mention that the surface finish in direct metal deposition is improved when the substrate surface is located at the focus plane of the powder stream [12, 13].

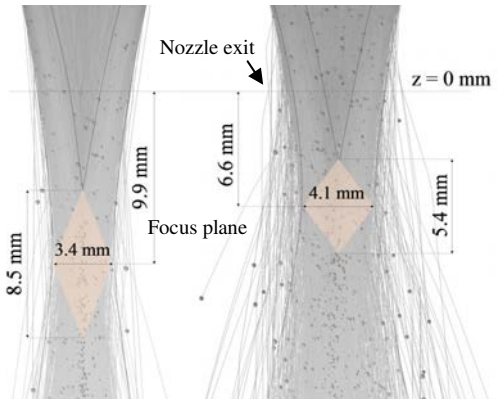

Figure 3. Particle stream structure obtained with Ti-6Al-4V (left) and 316L (right) alloys.

Figure 4 illustrates the velocity of the gas and powder particle calculated for Ti-6Al-4V. The substrate is a disk of 30 mm diameter and located at 4 mm from the nozzle exit. Due to the symmetry of the problem, only a quarter of the nozzle and substrate is modeled. It can be observed that the maximum gas velocity is reached at the exit of the channel containing the carrier gas and is 1.2 $m.s^{-1}$ whereas the maximum velocity of particle is 1.1 $m.s^{-1}$. The gas velocity drops down rapidly before it reaches the substrate.

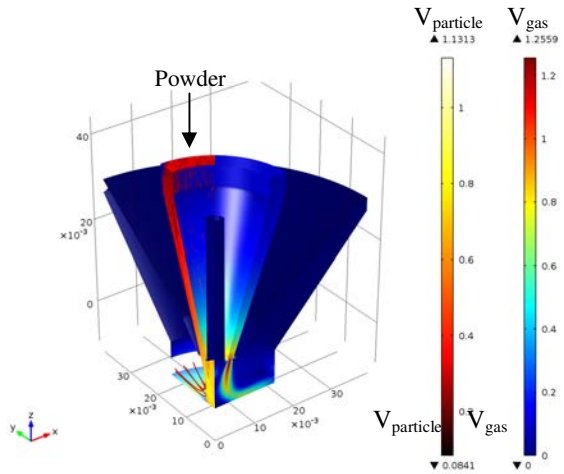

Figure 4. Velocity field and streamlines obtained for Ti-6Al-4V alloy.

Figure 5 compares the measured and modeled powder distributions at the substrate 4 mm below the nozzle exit. The powder distribution was measured by displacing a plate with a hole in a radial direction. The mass of the powder particles having crossed the hole is measured in order to determine the particle concentration profile.

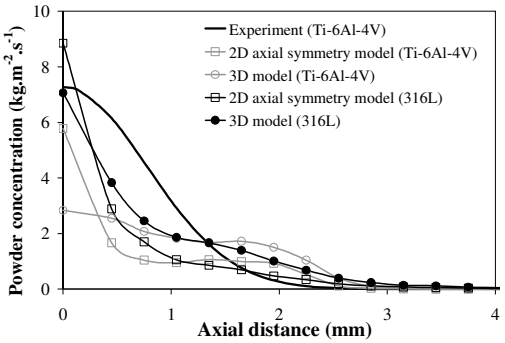

Figure 5. Measured and calculated particle concentration profiles at the substrate surface

The figure 5 compares also the numerical results obtained with the 3D model and a 2D axial symmetry model. The experimental results show clearly a Gaussian concentration distribution, which is less visible in the calculated results, especially for the Ti-6Al-4V alloy. This effect is due to the location of the substrate which is above the focus plane, as previously reported by Pinkerton [1]. It can be seen that the peak concentration values are greater with the 2D axial symmetry model than with the 3D model.

This is due to the 2D assumption which forces the particles to cross the axis. The concentration peak is then overestimated.

Figure 6 compares the calculated powder temperatures at the substrate surface obtained with both materials (Ti-6Al-4V and 316L) and two laser distributions (uniform and Gaussian).

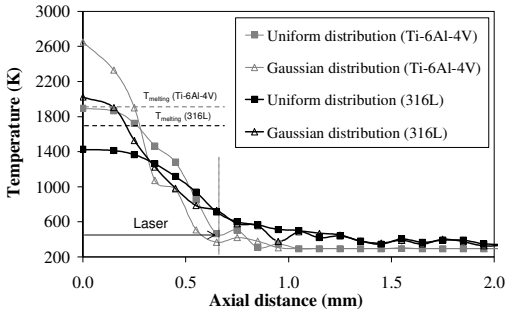

Figure 6. Calculated powder temperatures at the substrate surface for Ti-6Al-4V and 316L alloys using uniform or Gaussian laser distribution

For both materials, it is observed, as expected, a sharper temperature distribution with the Gaussian distribution. The peak temperatures are also higher for the Gaussian distribution and are above the melting point except for the stainless steel using a uniform temperature. It is worth to mention that the surface finish in direct metal deposition is better when the particles reaching the melt pool are melted.
Moreover, it can be noticed that the powder temperature of 316L steel is lower that the temperature of Ti-6Al-4V alloy near the axis but becomes higher far from the axis. The lower heating near the axis can be explained by the high thermal inertia of steel. However, the greater heating far from the axis is due to a longer interaction time between 316L particle and laser beam. As observed in Figure 3, some particles of 316L steel have a divergent trajectory at 4 mm from the nozzle exit. These particles interact with the laser beam during a longer time, inducing an excessive heating. This explains why some particles have a temperature higher than ambient temperature in the region away from the laser beam radius.

4. Conclusions

A numerical model that describes the dynamic and thermal behavior of the coaxial powder flow for direct metal deposition processes has been presented. The model accounts for phenomena of powder motion by gas drag and collisions with nozzle and substrate walls and thermal interactions between the powder stream and laser beam. This model is used to predict the location of the powder focus plane, which corresponds to the position where the substrate needs to be placed for an optimal deposition quality. Two materials are compared: a stainless steel 316L and a Ti-6Al-4V alloy. It has been shown that the focus point of the powder stream is located at a distance closer to the nozzle exit with the stainless steel. The heating of steel particles is lower at the center of the stream due to their inertia, but higher at the outers, because the interaction time with laser is greater. Two energy distributions of the laser beam have been analyzed. With a Gaussian distribution, the melting temperature is easily reached, compared to a uniform distribution, which leads to a more uniform temperature distribution. A good agreement between the numerical and experimental concentration profiles confirms that the model is capable of predicting the powder flow behaviour during the coaxial powder feeding of the direct metal deposition process.
The future development will take into account the collisions between particles and the laser beam attenuation due to powder stream. The coupling of this model with a melt pool model will also be considered in order to account for heat transfer from powder to melt pool and mass addition.

5. References

1. A.J. Pinkerton, “An analytical model of beam attenuation and powder heating during coaxial laser direct metal deposition”, *J. Phys. D: Appl. Phys.*, **40**, 7323-7334 (2007)
2. J. Lin, “Numerical simulation of the focused powder streams in coaxial laser cladding”, *J. Mater. Process. Tech.*, **105**, 17-23 (2000)
3. G. Zhu, D. Li, A. Zhang, Y. Tang, “Numerical simulation of metallic powder flow in a coaxial nozzle in laser direct metal deposition”, *Opt. Laser Technol.*, **43** (2011), 106-113

4. S. Zekovic, R. Dwivedi, R. Kovacevic, “Numerical simulation and experimental investigation of gas-powder flow from radially symmetrical nozzles in laser-based direct metal deposition”, *Int. J. Mach. Tool. Manu.*, **47**, 112-123 (2007)
5. J. Ibarra-Medina, M. Vogel, A.J. Pinkerton, “A CFD model of laser cladding: from deposition head to melt pool dynamics”, *Proc. ICALEO’2011*, Orlando, FL, USA, October 23-27 (2011)
6. I. Tabernero, A. Lamikiz, S. Martinez, E. Ukar, L.N. Lopez de Lacalle, “Modelling of energy attenuation due to powder flow-laser beam interaction during laser cladding process”, *J. Mater. Process. Tech.*, **212**, 516-522 (2012)
7. O.B. Kovalev, A.V. Zaitsev, D. Novichenko, I. Smurov, “Theoretical and experimental investigation of gas flows, powder transport and heating in coaxial laser Direct Metal Depositionn (DMD) process”, *J. Therm. Spray Techn.*, **20(3)**, 465-478 (2011)
8. S.Y. Wen, Y.C. Shin, J.Y. Murthy, P.E. Sojka, “Modeling of coaxial powder flow for the laser direct deposition process”, *Int. J. Heat Mass Tran.*, **52**, 5867-5877 (2009)
9. S. Morville, M. Carin, P. Peyre, M. Gharbi, D. Carron, P. Le Masson, R. Fabbro, 2D longitudinal modeling of heat transfer and fluid flow during multilayered DLMD process, *J. Laser Appl.*, **24** doi: 10.2351/1.4726445 (2012)
10. B. Wilthan, H. Reschab, R. Tanzer, W. Schützenhöfer, G. Pottlacher “Thermophysical properties of a Chromium-Nickel-Molybdenum steel in the solid and liquid phases”, *Int. J. Thermophys*., **29**, 434-444 (2008)
11. http://encyclopedia.airliquide.com/encyclopedia.asp
12. G. Pi, A. Zhang, G. Zhu, D. Li, B. Lu, “Research on the forming process of three-dimensional metal parts fabricated by laser direct metal forming”, *Int. J. Adv. Manuf. Technol*., **57**, 841-847 (2011)
13. G. Zhu, D. Li, A. Zhang, G. Pi, Y. Tang, “The influence of laser and powder defocusing characteristics on the surface quality in laser direct deposition”, *Optics & Laser Technology*, **44**, 349-356 (2012)

6. Acknowledgements

This work is supported by the French National Research Agency (ANR), under ASPECT project No. ANR-09-BLAN-0014-02.